The SAMI Galaxy Survey: the discovery of a luminous, low-metallicity H II complex in the dwarf galaxy GAMA J141103.98−003242.3

S. N. Richards,[1,2,3]★ A. L. Schaefer,[1,2,3] Á. R. López-Sánchez,[2,4] S. M. Croom,[1,3]
J. J. Bryant,[2,3] S. M. Sweet,[5] I. S. Konstantopoulos,[2] J. T. Allen,[1,3] J. Bland-Hawthorn,[1]
J. V. Bloom,[1,3] S. Brough,[2] L. M. R. Fogarty,[1,3] M. Goodwin,[2] A. W. Green,[2]
I. -T. Ho,[6] L. J. Kewley,[7] B. S. Koribalski,[8] J. S. Lawrence,[2]
M. S. Owers,[2] E. M. Sadler[1,3] and R. Sharp[3,6]

[1]*Sydney Institute for Astronomy, School of Physics, University of Sydney, NSW 2006, Australia*
[2]*Australian Astronomical Observatory, PO Box 915, North Ryde, NSW 1670, Australia*
[3]*CAASTRO: ARC Centre of Excellence for All-sky Astrophysics*
[4]*Department of Physics and Astronomy, Macquarie University, NSW 2109, Australia*
[5]*School of Mathematics and Physics, University of Queensland, QLD 4072, Australia*
[6]*Institute for Astronomy, University of Hawaii, 2680 Woodlawn Drive, Honolulu, HI 96822, USA*
[7]*Research School of Astronomy and Astrophysics, Australian National University, Cotter Rd., Weston, ACT 2611, Australia*
[8]*Australia Telescope National Facility, CSIRO Astronomy and Space Science, PO Box 76, Epping NSW 1710, Australia*

ABSTRACT

We present the discovery of a luminous unresolved H II complex on the edge of dwarf galaxy GAMA J141103.98−003242.3 using data from the Sydney-AAO Multi-object Integral field spectrograph (SAMI) Galaxy Survey. This dwarf galaxy is situated at a distance of ∼100 Mpc and contains an unresolved region of H II emission that contributes ∼70 per cent of the galaxy's Hα luminosity, located at the top end of established H II region luminosity functions. For the H II complex, we measure a star formation rate of 0.147 ± 0.041 M$_\odot$ yr^{-1} and a metallicity of 12+log(O/H) = 8.01 ± 0.05 that is lower than the rest of the galaxy by ∼0.2 dex. Data from the H I Parkes All-Sky Survey (HIPASS) indicate the likely presence of neutral hydrogen in the galaxy to potentially fuel ongoing and future star-forming events. We discuss various triggering mechanisms for the intense star formation activity of this H II complex, where the kinematics of the ionized gas are well described by a rotating disc and do not show any features indicative of interactions. We show that SAMI is an ideal instrument to identify similar systems to GAMA J141103.98−003242.3, and the SAMI Galaxy Survey is likely to find many more of these systems to aid in the understanding of their formation and evolution.

Key words: techniques: spectroscopic – H II regions – galaxies: dwarf – galaxies: evolution – galaxies: starburst – galaxies: star formation.

1 INTRODUCTION

Galaxies are thought to have formed hierarchically from the agglomeration of smaller structures. While dwarf galaxies (DGs) occupy the lower end of the galaxy mass function, they are a critical population for the understanding of galaxy evolution as they represent the fundamental units of galaxy formation in the early Universe. Over the years there have been varying definitions as to what is classified as a DG (Hodge 1971; Tammann 1994; Mateo 1998). For the purpose of this work, we define a DG as a galaxy with a stellar mass $<10^9$ M$_\odot$. Despite DGs being the most numerous galaxies in the Universe (Fontana et al. 2006), their low stellar masses frequently result in a low surface brightness. Due to the *Malmquist bias*, extensive studies of DGs have therefore only been carried out in the Local Group (e.g. Hunter, Hawley & Gallagher 1993; Mateo 1998; Begum et al. 2008; Tolstoy, Hill & Tosi 2009) and within the Local Volume (e.g. Kennicutt et al. 2008; Kirby et al. 2008; Bouchard, Da Costa & Jerjen 2009; Dalcanton et al. 2009; Young et al. 2014). Few analyses of DGs extend beyond ∼10 Mpc

distance. These studies have been typically focused on Blue Compact Dwarf galaxies (BCDGs; Gil de Paz, Madore & Pevunova 2003; Izotov & Thaun 2004; López-Sánchez & Esteban 2008; Cairós et al. 2009; Hunter, Elmegreen & Ludka 2010; Karthick et al. 2014) that show intense star-forming knots within a clumpy Hα morphology. Analyses of H II regions in DGs are important for understanding their star formation history (SFH). Observationally, emission-line diagnostics (e.g. Kewley & Dopita 2002; Dopita et al. 2006, 2013) or theoretical evolution synthesis models (e.g. Leitherer et al. 1999; Bruzual & Charlot 2003; Mollá, García-Vargas & Bressan 2009) can be used to constrain the physical parameters of extragalactic H II regions and their host galaxies.

The Hα luminosity function of H II regions in BCDGs covers the range 10^{36}–10^{41} erg s^{-1}, and seems to follow those of larger nearby galaxies (Oey & Clarke 1998; Youngblood & Hunter 1999; Bradley et al. 2006). H II regions with Hα luminosities on the order of $>10^{40}$ erg s^{-1} (the top percentile of the H II region luminosity function) are of particular interest as they are the hosts of the most extreme star formation events, which drive the evolution of galaxies. For comparison, the famous H II complex 30 Doradus (NGC 2070) in the Large Magellanic Cloud (LMC) has an Hα luminosity of 1.5×10^{40} erg s^{-1} (Kennicutt 1984), a metallicity of $12+\log(\mathrm{O/H}) = 8.33 \pm 0.02$ (Peimbert 2003), and it is currently forming a massive star cluster (Bosch, Terlevich & Terlevich 2009). SBS 0335−052E, II Zw 40 and J1253−0312 (Pustilnik, Pramskij & Kniazev 2004; Moustakas & Kennicutt 2006; Guseva et al. 2011) are BCDGs that occupy the very extreme end of the H II region luminosity function with Hα luminosities $>10^{41}$ erg s^{-1}. In a massive star cluster the first supernovae will occur roughly a million years after the initial burst of star formation and may expel a large fraction of the gas within. Therefore, a sustained star formation rate (SFR) of the order of 0.1 M$_\odot$ yr^{-1} is required for the formation of a cluster of $\sim 10^5$ M$_\odot$.

Some works have shown that galaxy interactions trigger strong star formation activity in DGs (e.g. Koribalski & López-Sánchez 2009). The multiwavelength analysis of BCDGs performed by López-Sánchez (2010) found that the majority of them were clearly interacting or merging with low-luminosity dwarf objects or H I clouds. The interacting features were only detected by deep optical spectroscopy and detailed multiwavelength analysis, which includes a study of the kinematics and distribution of the neutral gas. Indeed, many times the disturbances were found when examining the neutral gas, as was the case in the DGs NGC 1705 (Meurer et al. 1998), NGC 625 (Cannon et al. 2004), NGC 1569 (Mühle et al. 2005), IC 4662 (van Eymeren et al. 2010) and NGC 5253 (López-Sánchez et al. 2012a). This is often the case because low mass companions often have a high gas fraction and are therefore visible in H I emission. Moreover, aperture synthesis observations of spectral lines are usually performed at high spectral resolution, allowing kinematic maps of these sources to be produced. An example of a merger-induced star formation event in a dwarf system is SBS 1319+579 (López-Sánchez & Esteban 2009), where long slit spectroscopy revealed differing velocity components for the merging systems.

Luminous H II regions can also be created stochastically by processes internal to a galaxy. For example, star formation could be triggered either by density waves propagating through an irregular distribution of H I (Gerola, Seiden & Schulman 1980) or solely by the gravitational collapse of a gas cloud within the galaxy disc (Lada et al. 2008). Bauer et al. (2013) analysed the SFRs and specific-SFRs (SSFRs) of low-mass ($<10^{10}$ M$_\odot$) galaxies within the GAMA-I survey and concluded that their SFHs require stochastic bursts of

star formation superimposed on to an underlying exponentially declining SFH. This is enhanced in low-mass galaxies as they have fewer individual star-forming regions compared to more massive galaxies (Lee et al. 2009).

Clumpy star-forming galaxies at higher redshift ($z \sim 1$–2), so-called 'clump-clusters' (Elmegreen, Elmegreen & Hirst 2004), host star-forming clumps (regions) with diameters on the scale of a few kpc (Wisnioski et al. 2012). Local dwarf-irregular galaxies have been used as analogues for these higher redshift galaxies, as they can be seen as currently undergoing the same evolutionary phase. The difference is the time-scale over which these large star-forming regions and the host galaxy evolve, inversely proportional to their stellar mass. Today most of these clump-clusters have evolved into smooth discs, leaving dwarf irregulars as a visible example of this phase (Elmegreen et al. 2009).

Observationally, extragalactic H II regions are best identified with spatially resolved spectroscopy or emission-line imaging. Broadband photometry using $g - r$ versus $r - i$ colour–colour diagrams (Cardamone et al. 2009; Izotov, Guseva & Thuan 2011) or narrowband Hα imaging can be used to identify H II regions with strong emission lines, but they are unable to obtain line ratios and velocity information. Integral field spectroscopy (IFS), on the other hand, can trace dynamics, metallicities and gas processes through line velocities and abundances, which can help to identify the triggers for star formation. Besides some analyses of individual objects (e.g. James et al. 2009; James, Tsamis & Barlow 2010; Monreal-Ibero et al. 2010; López-Sánchez et al. 2011; Pérez-Montero et al. 2011), few IFS surveys, with the exception of the *Small Isolated Gas Rich Irregular Dwarf galaxy survey* (SIGRID; 83 DGs; Nicholls et al. 2011), the *IFS – Blue Compact Galaxy survey* (IFS-BCG; 40 DGs; Cairós et al. 2012), and the *Choirs survey* (Choirs, 38 DGs; Sweet et al. 2013), have been targeting DGs. As all of these works used a single Integral Field Unit (IFU) instrument, the time taken to gather their data has been lengthy. The quoted number of targets for each survey is the proposed quantity, with no survey complete at the time of writing.

The Sydney-AAO Multi-object Integral field spectrograph (SAMI) Galaxy Survey (Croom et al. 2012; Allen et al. 2014; Bryant et al. 2014b; Sharp et al. 2014), which uses the SAMI, deployed at prime focus on the 3.9-m Anglo-Australian Telescope (AAT), started observations in early 2013, and seeks to obtain spatially resolved spectra for ~ 3400 galaxies over 3 years. This survey has the ability to identify and analyse H II complexes in galaxies with a large range of stellar masses [$7.4 \lesssim \log(\mathrm{M/M_\odot}) \lesssim 12.7$]. The survey has a number of overlapping volume-limited samples with different stellar mass and redshift limits [see Bryant et al. (2014b) for details of the target selection]. Consequently ~ 400 galaxies in the sample will have stellar masses $<10^9$ M$_\odot$. Upon visually checking 70 DGs that have already been observed with SAMI, GAMA J141103.98−003242.3 stood out due to an unusually luminous H II complex located at the edge of the galaxy, which was strikingly visible in its Hα map, but barely seen in the continuum maps. This galaxy and its luminous H II complex are the focus of the work presented here.

In Section 2 we present existing data on GAMA J141103.98−003242.3; in Section 3 we describe the SAMI observations that are the focus of this paper; in Section 4 we detail measurements made from the SAMI data; in Section 5 we discuss likely mechanisms that are driving the evolution of GAMA J141103.98−003242.3. In this paper we assume the standard Λcold dark matter cosmology with $\Omega_m = 0.3$, $\Omega_\Lambda = 0.7$ and $H_0 = 73$ km s^{-1} Mpc^{-1}.

Table 1. Derived properties for GAMA J141103.98−003242.3 and its bright H II complex. Values in the upper section of the table have been derived from previous studies. The values in the lower half of the text have been derived from the SAMI data cube as described in the text. M_{stars} is stellar mass, M_{gas} is neutral gas mass (including helium), M_{bar} is baryonic mass, M_{dyn} is dynamical mass, $M_{H II}$ is ionized gas mass and $M_\star$ is stellar ionizing cluster mass. 'Rest of the galaxy' excludes the H II complex.

GAMA 567676 = GAMA J141103.98−003242.3		
RA (J2000)	14:11:03.98	
Dec. (J2000)	−00:32:42.39	
z	0.0259	
d (Mpc)	106	
R_e	4.3 arcsec = 1.5 kpc	
i (°) †	∼35	
$\log(M_{stars}/M_\odot)$	8.52 ± 0.13	
$\log(M_{gas}/M_\odot)$	∼9.62	
$\log(M_{bar}/M_\odot)$	∼9.66	
M_{gas}/M_{stars}	∼11.2	
$v_{rot,HI}$ (km s^{-1})	∼55	
$\log(M_{dyn}/M_\odot)$	∼9.74	
Hα-SFR (M$_\odot$ yr^{-1}) (GAMA)	0.121	
FUV-SFR (M$_\odot$ yr^{-1})	0.58 ± 0.24	
	H II complex	Rest of the galaxy
EW(Hα) (Å)	451 ± 11	34.8 ± 3.2
EW(Hβ) (Å)	137 ± 4	6.8 ± 1.6
F(Hα) (10^{-16} erg s^{-1} cm^{-2}) ‡	138 ± 38	54 ± 15
L(Hα) (10^{39} erg s^{-1})	18.5 ± 5.2	7.3 ± 2.0
$\log(M_{H II}/M_\odot)$	5.58 ± 0.11	5.02 ± 0.11
$\log(M_\star/M_\odot)$	5.81	6.53
Equivalent O7V stars	1360	538
Age of most recent starburst (Myr)	4.8 ± 0.2	7.9 ± 0.4
$E(B-V)$ (mag)	0.24 ± 0.01	0.21 ± 0.04
12+log(O/H)	8.01 ± 0.05	8.18 ± 0.11
log(N/O)	−1.43 ± 0.06	−1.51 ± 0.10
Hα-SFR (M$_\odot$ yr^{-1})	0.147 ± 0.041	0.058 ± 0.016

†Derived from the ellipticity on GAMA's Sérsic fit to the *r*-band photometry.
‡Error is currently dominated by a 28 per cent error in SAMI's absolute flux calibration, and in all values derived from it [see Allen et al. (2014) for more details].

2 EXISTING DATA ON GAMA J141103.98−003242.3

In this section we introduce the properties of GAMA J141103.98−003242.3 as determined by prior observations. It was observed by GAMA (Driver et al. 2011; Hopkins et al. 2013), who find a spectroscopic redshift of $z = 0.0259$ (106 Mpc), and from the Sloan Digital Sky Survey (SDSS) photometry find a Sérsic radius of 4.26 arcsec (1.98 kpc; Kelvin et al. 2012) and a stellar mass of $\log(M_{stars}/M_\odot) = 8.52 ± 0.13$ (Taylor et al. 2011).

The main properties of this galaxy are tabulated in Table 1. GAMA also calculates an aperture-corrected SFR of 0.121 M$_\odot$ yr^{-1} (Gunawardhana et al. 2013). SDSS optical (Petrosian *r*-band magnitude of 18.16; Abazajian et al. 2009) and *GALEX* UV photometry (Morrissey et al. 2007) are also available for this galaxy. The measured *FUV* magnitude and *FUV–NUV* colour are 20.63 ± 0.05 and 0.29 ± 0.05, respectively, and applying the Salim et al. (2007) calibration to their respective fluxes, a *FUV*-based SFR of 0.58 ± 0.24 M$_\odot$ yr^{-1} is found.

This galaxy has a 4σ detection of the H I 21-cm line using the H I Parkes All-Sky Survey (HIPASS; Barnes et al. 2001) measured
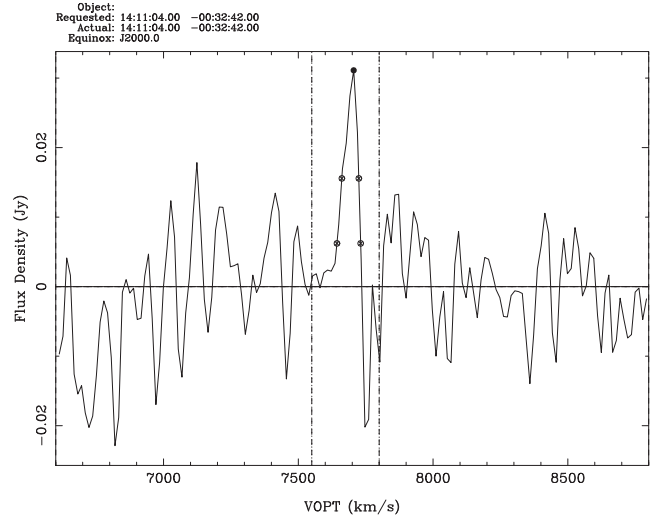
Figure 1. The HIPASS radio spectrum in the direction of GAMA J141103.98−003242.3. This spectrum shows evidence for a 21 cm neutral hydrogen emission feature at the redshift of the galaxy with a flux of 1.4 Jy km s^{-1} (central dot), a 50 per cent velocity width of 63 km s^{-1} (inner two dots), and an 80 per cent velocity width of 88 km s^{-1} (outer two dots). The full width at half-maximum (FWHM) of the Parkes gridded beam is 15.5 arcmin. The typical *rms* noise in HIPASS is 13 mJy beam^{-1}. The measured H I peak flux is ∼2.5 σ, the integrated flux is ∼4 σ. The HIPASS channel width is 13.2 km s^{-1}; the velocity resolution is 18 km s^{-1}. VOPT is the velocity scale of the HIPASS data with respect to the solar barycentre in the usual optical (*cz*) convention.

over multiple channels, as shown in Fig. 1. This translates into an H I mass of $\log(M_{H I}/M_\odot) \sim 9.50$ and a 50 per cent velocity width of 63 km s^{-1}. Neglecting the molecular gas (which is expected to be very low in low-metallicity galaxies), and accounting for helium (25 per cent), the total neutral gas mass is $\log(M_{gas}/M_\odot) \sim 9.62$. Hence, the baryonic mass is $\log(M_{bar}/M_\odot) \sim 9.66$ and the gas-to-stellar mass ratio $M_{gas}/M_{stars} \sim 11.2$. Assuming that the motion of the neutral gas is due to disc rotation and considering an apparent inclination angle of $i \sim 35°$ (as measured from the ellipticity values from the GAMA Sérsic fit), we estimate a maximum rotational velocity amplitude of $v_{rot,HI} \approx 55$ km s^{-1}. Considering that the neutral gas may be extended at least up to four times the optical size of the galaxy (4 × R_e = 7.9 kpc; e.g. Warren, Jerjen & Koribalski 2004), this yields to a total dynamical mass of $\log(M_{dyn}/M_\odot) \sim 9.74$. Therefore, this DG possesses at least a mass of $\log(M/M_\odot) \sim 8.97$ in the form of dark matter. It should be noted that the HIPASS beam FWHM is 15 arcmin. However, given that the redshift of the H I detection closely matches the optical redshift of the galaxy ($v_{opt} = 7765$ km s^{-1}, $v_{HI} \approx 7675$ km s^{-1}) and that there are no catalogued galaxies at the same redshift, it is highly likely that the detected neutral gas is associated with GAMA J141103.98−003242.3.

3 OBSERVATIONS AND DATA REDUCTION

The data on which this analysis is based were obtained with the SAMI instrument. SAMI deploys 13 hexabundles (Bland-Hawthorn et al. 2011; Bryant et al. 2014a) over a 1° field at the Prime Focus of the AAT. Each hexabundle is made up of 61 optical fibres, circularly packed, with each having a core size of 1.6 arcsec, resulting in a hexabundle field of view (f.o.v) of 15 arcsec diameter. All 819 fibres

(793 object fibres and 26 sky fibres) feed into the AAOmega spectrograph (Sharp et al. 2006), configured to a wavelength coverage of 370–570 nm with $R = 1730$ in the blue arm, and 625–735 nm with $R = 4500$ in the red arm. 12 galaxies are observed in one pointing, along with a secondary standard star that is used for telluric correction and PSF sampling. All frames have a flux zero-point respective to a stand-alone primary standard star observation in one of the bundles, meaning variable sky conditions between the primary standard star observation and the galaxy frames are not taken into account. Due to this, in addition to SAMI's data reduction pipeline, which is still in development, preliminary absolute flux calibration is found to be consistent across the survey data set to ~6 per cent. However, a residual baseline offset uncertainty between frames taken in variable conditions is not yet accounted for and hence we estimate a 28 per cent uncertainty in this early survey data (see Allen et al. 2014, for more details).

GAMA J141103.98−003242.3 was observed using SAMI on 2013 March 15, with some high-level clouds, and a seeing of ~2 arcsec. A seven-point dither was performed to achieve near-uniform spatial coverage, with 1800 s exposure time for each frame, totalling 3.5 h.

The raw data were reduced using the AAOmega data reduction pipeline, 2DFDR,[1] followed by full alignment and calibration through the SAMI Data Reduction pipeline (see Sharp et al. 2014, for a detailed explanation of this package). The resulting product of SAMI-DR is a data cube for each of the blue and red observations, both of which have been flux calibrated and corrected for differential atmospheric refraction.

To obtain the line, velocity and velocity dispersion maps of each galaxy (subtracted for instrumental broadening), the reduced cubes were fitted using a new IFU line fitting package called LZIFU (see Ho et al., in preparation for a detailed explanation of this package). This software makes use of the pPXF (Cappellari & Emsellem 2004) stellar template fitting routine as well as the MPFIT library (Markwardt 2009) for estimating emission line properties. LZIFU has the ability to perform multicomponent Gaussian fits to each emission line, though in the case of GAMA J141103.98−003242.3 only a single component was fitted as a multicomponent fit did not give a significant improvement in the reduced chi-squared. It was from the product of LZIFU that this system was identified. To perform detailed analysis, IRAF[2] software was used to analyse the summed, aperture-extracted 1D spectra. Line fluxes and equivalent widths were measured by integrating all the flux in the line between two given limits and over a local continuum estimated by visual inspection of the spectra. Visual inspection of the spectra is needed to get a proper estimation of the adjacent continuum and hence a reliable line flux estimation when emission lines are faint. The errors associated with the line flux measurements were estimated by remeasuring the noise (*rms*) in the adjacent continuum of each emission line.

4 RESULTS

The products of LZIFU give spatially resolved information regarding the distribution of ionized gas in GAMA J141103.98−003242.3. From the data collected, maps were generated of the Hα, Hβ, [N II]

---

[1] 2DFDR is a public data reduction package managed by the Australian Astronomical Observatory (see http://www.aao.gov.au/science/software/2dfdr).
[2] IRAF (*Image Reduction and Analysis Facility*) is distributed by NOAO which is operated by AURA Inc., under cooperative agreement with NSF.

λ 6583, [O III] λ 5007 and [O II] λ 3727 distribution, as well as the line-of-sight velocity field; these are displayed in Fig. 2. A bright emission region, located ~5.1 arcsec (1.2 $R_e = 2.6$ kpc) north-west of the galaxy centre, clearly appears in the Hα map – at the same velocity as the galaxy. This is interpreted as an off-centre, luminous star-forming complex within the DG. A two-dimensional Gaussian fit to the H II complex in the SDSS *r*-band image gives a FWHM of 1.2 arcsec. This places an upper limit of ~600 pc on its diameter, implying that the H II complex is unresolved by both SDSS and the SAMI Galaxy Survey.

From the emission line fits, we are able to produce maps of the velocity and velocity dispersion in the interstellar medium of GAMA J141103.98−003242.3. These maps are displayed in Fig. 2. The gas velocity map is typical of a disc rotating about a north-west–southeast axis with a maximum amplitude of approximately 25 km s^{-1}, which is approximately half of the $v_{\rm rot,H\,I}$ estimated from the 21-cm H I line. The velocity map displays a smooth gradient across the entire f.o.v, suggesting that the H II complex is corotating with the galaxy.

Areas of the data cube corresponding to the H II complex and the remainder of the galaxy were binned to obtain measurements with reduced random errors. A circle of radius 2 arcsec, centred on the peak of the Hα intensity, was used to delimit the zone of the cube regarded as part of the H II complex. The binned spectrum of the H II complex and the rest of the galaxy are shown in Fig. 3, with all emission lines measurements performed manually (as discussed in Section 3).

In the binned spectrum of the H II complex we also detect emission lines of He I, He II, [O I], [S II], [S III], [Ne III], [Ar III] and [Ar IV], as well as the auroral [O III] λ 4363 line and many H I Balmer lines. The complete list of emission lines detected is shown in Table A1, which also includes the dereddened line intensity ratios with respect to $I(H\beta)=100$. The presence of high-excitation ions such as [Ar IV] or He II indicates the high degree of ionization of the gas. We have followed the same prescriptions described in López-Sánchez & Esteban (2009) to determine the physical conditions (electron density, electron temperature, ionization degree, and reddening) and chemical abundances of this H II complex. The reddening coefficient, $c(H\beta)$, was computed using three pairs of H I Balmer lines assuming their theoretical ratios for case B recombination given by Storey & Hummer (1995) and a Cardelli, Clayton & Mathis (1989) extinction law. We assume the same $W_{\rm abs}$ for all Balmer lines and contributions other than extinction and stellar absorption are negligible, with both $W_{\rm abs}$ and $c(H\beta)$ being simultaneously optimized to best match the observed Balmer pair ratios. A full description of this method is given in Mazzarella & Boroson (1993) and López-Sánchez & Esteban (2009). This method, applied to each detectable Balmer line, provides a consistent value of $c(H\beta) = 0.34 \pm 0.02$. The electron density, computed via the [S II] λλ 6716, 6731 doublet, is $n_e = 140 \pm 30$ cm^{-3}.

The detection of the [O III] λ 4363 line allows us to compute the electron temperature via the [O III] (λ 4959+λ 5507)/λ 4363 ratio, $T_e([O\,III])=14000 \pm 650$ K. We then assumed a two-zone approximation to define the temperature structure of the nebula, using $T_e([O\,III])$ as representative of high-ionization potential ions. The electron temperature assumed for the low-ionization potential ions was derived from the linear relation between $T_e([O\,III])$ and $T_e([O\,II])$ provided by Garnett (1992). We finally derived the ionic and total abundances of O, N, S, Ar and Ne, as well as the N/O, S/O, Ar/O and Ne/O ratios, for this H II complex following the direct method. The results are compiled in Table A2. In particular, we find a very high excitation degree in the gas, log (O^{++}/O$^+$) = 0.78 ± 0.09, and
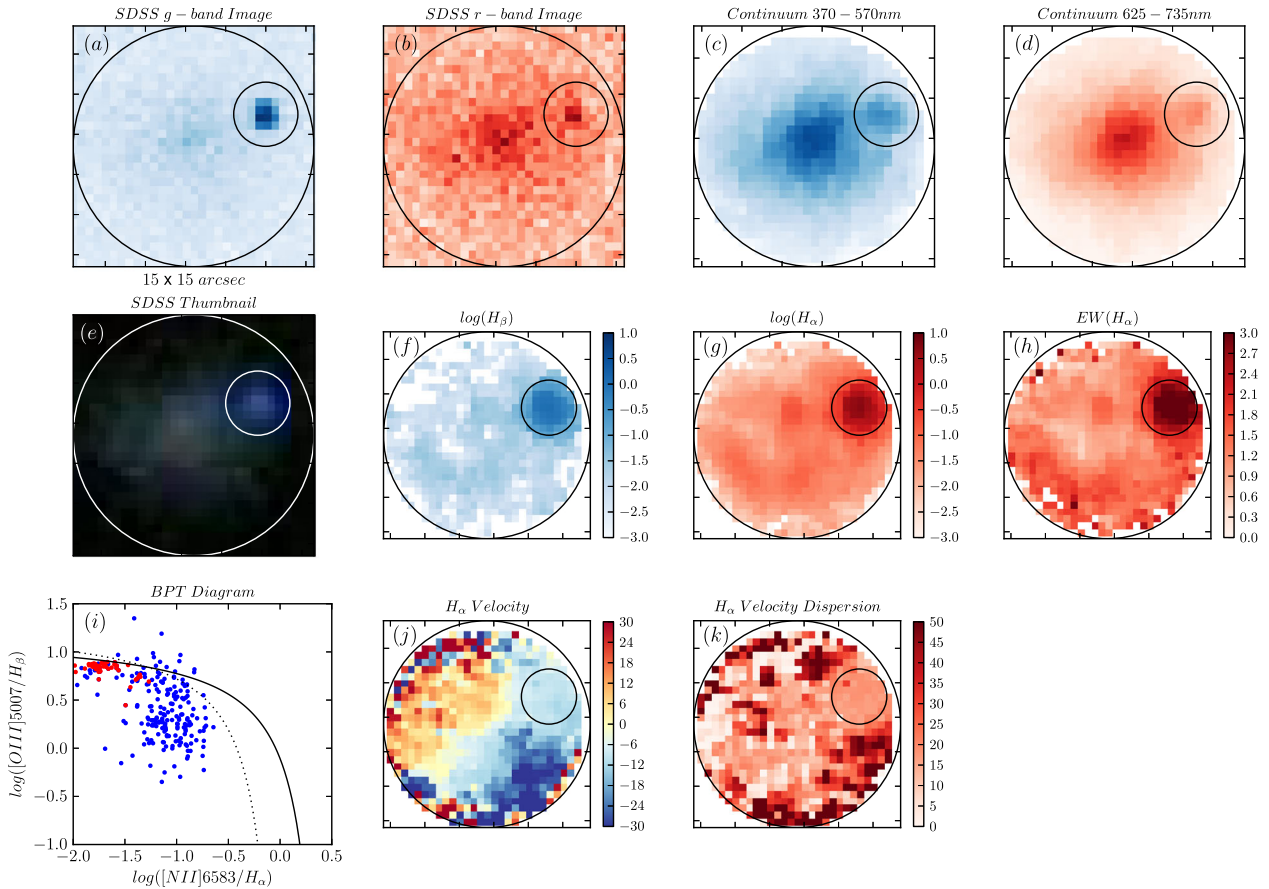
Figure 2. Diagnostic plots for GAMA J141103.98−003242.3. (a) and (b): the SDSS *g*- and *r*-band images. (c) and (d): the LZIFU fitted continuum maps. (e): the SDSS three-colour thumbnail. (f) and (g): the Hβ and Hα maps, respectively (normalized to 10^{-16} erg s^{-1} cm^{-2}). (h): the log(EW(Hα)) map in units of Å. (i): the BPT diagram where the spaxels are colour-coded such that the red points are the spaxels within the H II complex, and the blue spaxels are the rest of the galaxy. The black solid and dotted lines represent the star formation limits as prescribed by Kewley et al. (2001) and Kauffmann et al. (2003), respectively. (j): the Hα velocity field in km s^{-1}. (k): the Hα velocity dispersion in km s^{-1}. In all images, the box is 15×15 arcsec (0.5-arcsec per pixel), the large black circle enclosing the galaxy has a diameter of 15 arcsec, and the small black circle (centred about the H II complex) has a diameter of 4 arcsec. In all images, north is up and east is left.

derive 12+log(O/H) = 8.01 ± 0.05 and log(N/O) = −1.43 ± 0.06. These values are typical for H II regions in BCDGs (e.g., Izotov & Thuan 1999; Izotov et al. 2004; López-Sánchez & Esteban 2010).

We have combined all of the spaxels of the galaxy, excluding those belonging to the H II complex, to quantify its global extinction and metallicity. However, now only the brightest emission lines are detected (see Table A1), and hence we have to resort to strong-line methods (SEL) to determine the oxygen abundance of the gas. Table A3 compiles the results for the metallicity of the ionized gas following the most common SEL techniques. For comparison, Table A3 also lists the oxygen abundance derived in the H II complex following the same empirical methods. Besides the problem of the absolute abundance scale (see López-Sánchez et al. 2012b, for details), it is clear that the H II complex has oxygen abundances which are systematically ∼0.2 dex lower than those observed in the rest of the galaxy. Assuming an oxygen abundance of 12+log(O/H) = 8.18 (the average obtained using the T_e-based SEL methods), we computed electron temperatures, ionic and total abundances for the rest of the galaxy, which are compiled in Table A2. Using the same method as used on the H II complex, for the rest of the galaxy we calculate c(Hβ) = 0.31 ± 0.04 and W_{abs} = 0.8 ± 0.2 Å.

72 per cent of all the Hα emission of GAMA J141103.98− 003242.3 is found in the H II complex. Using the extinction-

corrected Hα flux we derive a total Hα luminosity of (18.5 ± 5.2) $\times 10^{39}$ erg s^{-1} for the H II complex. Applying the Kennicutt (1998) relationship under the assumption of a Salpeter (1955) stellar initial mass function, we estimate a SFR of 0.147 ± 0.041 M$_\odot$ yr^{-1}. Using an O7V Hα luminosity of 1.36×10^{37} erg s^{-1} from Schaerer & Vacca (1998), the number of equivalent O7V stars needed to explain the Hα luminosity is 1360; similar to the number estimated for 30 Doradus (Doran et al. 2013). Using prescriptions from Díaz (1998), the mass of ionized gas, log ($M_{H II}$/M$_\odot$) = 5.58 ± 0.11, and the mass of the stellar ionizing cluster, log ($M_\star$/M$_\odot$) = 5.81, also matches those values found in 30 Doradus (Faulkner 1967; Bosch et al. 2009). Assuming an instantaneous burst with $Z = 0.008$ and considering the Starburst 99 models (Leitherer et al. 1999), the Hα equivalent width indicates that the last star formation event in this H II complex happened 4.8 Myr ago. These values are tabulated in Table 1.

The combined Hα-SFR of the galaxy including the H II complex is 0.21 ± 0.06 M$_\odot$ yr^{-1}, which is higher than that measured by GAMA, though lower than the *FUV*-SFR measured from *GALEX*. It has been observed that the *FUV*-SFR is usually higher than the Hα-SFR in DGs (e.g. Lee et al. 2009). The discrepancy with the GAMA SFR could be explained by an inadequate aperture correction, as a 2 arcsec fibre
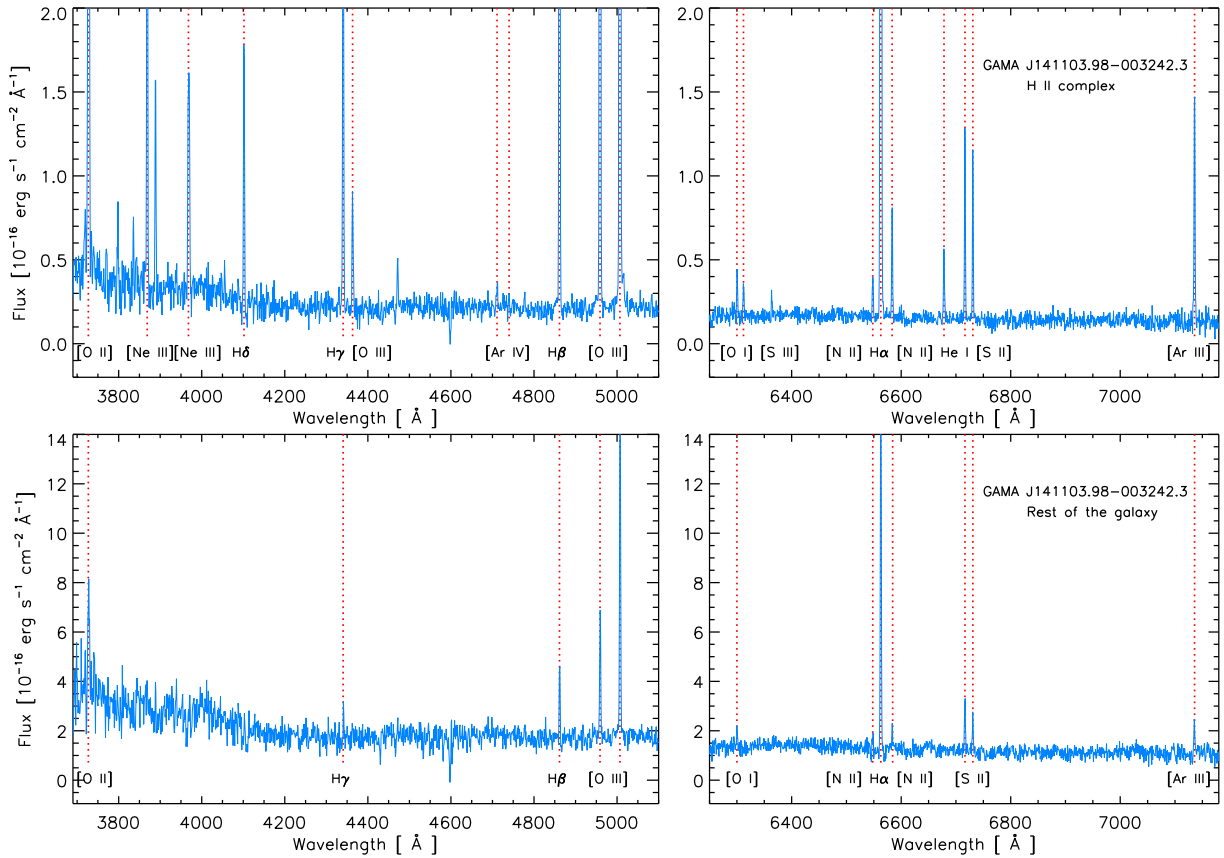
Figure 3. Binned optical spectrum of the H II complex (top) and the rest of the galaxy (bottom) using SAMI data. 'Rest of the galaxy' excludes the H II complex. The main emission lines are identified by red dotted lines. The wavelength scale is expressed in the rest frame of the galaxy. The red spectrum only shows the $\lambda\lambda$ 6250–7175 range. Note that the flux scales in both the blue and red spectra have been truncated in order to accentuate the weaker emission lines.

aperture placed on GAMA J141103.98−003242.3 would miss its H II complex.

5 DISCUSSION AND CONCLUSIONS

The analysis of GAMA J141103.98−003242.3 has revealed a luminous H II complex with a SFR high enough to create a massive star cluster. This system has interesting implications for our understanding of DG star formation and evolution in the Local Universe. This galaxy is both visually and spectroscopically similar to the LMC-30 Doradus system, in hosting a single dominant star-forming region in the outer disc, and in many ways could be considered as a more distant analogue of one of our nearest neighbours.

Off-centred bright star-forming regions are often found in BCDGs (e.g. Loose & Thuan 1986; Cairós et al. 2001; Gil de Paz et al. 2003; López-Sánchez & Esteban 2008), but as we have shown in this paper, with IFU data we obtain detailed chemical and kinematic information. This allows us to probe the physical mechanisms that can explain the presence of this H II complex in GAMA J141103.98−003242.3, either by external triggering or by the intrinsic stochasticity of star formation in an undisturbed system. With the data available there is no indication that the onset of star formation has been induced by an interaction with a companion. In particular, there appear to be no kinematic disturbances in the ionized gas in the galaxy. The smooth kinematic distribution and low velocity dispersion at the location of the H II complex are suggestive of the fact that it is located in an undisturbed, rotationally supported disc.

The main difference between GAMA J141103.98−003242.3 and the LMC is its isolation. GAMA assigns it one companion, GAMA J141120.29−002950.8, which is ∼5 arcmin to the north-east and a physical separation of ∼4 Mpc. There is no other catalogued companion (GAMA or SDSS) within 300 km s⁻¹ and a 20 arcmin radius of GAMA J141103.98−003242.3. Visual inspection of optical (SDSS, $r \lesssim 23$) and NIR (2MASS, $K_s \lesssim 13.5$) imaging for this region revealed no indication of companion galaxies similar to or larger than GAMA J141103.98−003242.3.

The HIPASS data revealed a significant amount of H I in the vicinity of GAMA J141103.98−003242.3, indicating $M_{gas}/M_{stars} \sim$ 11.2, with $\log(M_{H I}/M_{\odot}) \sim 9.5$ [LMC $\log(M_{H I}/M_{\odot}) \sim 8.7$; Brüns et al. 2005. Thus, the galaxy potentially has access to a large reservoir of neutral gas. The apparent lower metallicity of the H II complex may suggest that the gas feeding the star formation has fallen in from the outer parts of the H I disc following its expulsion during a previous episode of activity. Alternatively, the gas may have been supplied by an interaction with a companion galaxy as has been seen previously in other DG systems (e.g. López-Sánchez et al. 2012a), although the gas fraction with respect to the stellar mass and metallicity is not abnormal for similar galaxies (Huang et al. 2012; Hughes et al. 2013). A lower mass companion that is less obvious could play a part, as seen in Tol 30 where an H I tail extends towards a smaller DG (López-Sánchez et al. 2010, López-Sánchez et al., in preparation). With no obvious companion near GAMA J141103.98−003242.3, and the fact that any galaxy too faint to be detected in the SDSS image would have an even more extreme gas/star ratio, the origin of the H I gas from a previous

interaction is both unlikely and unnecessary. Only with resolved H I mapping of the region around GAMA J141103.98−003242.3 can a conclusion of its role on the H II complex be made.

The use of the term 'H II complex' in this work highlights the unresolved nature of this region, which warrants caution when deriving physical quantities. Pleuss, Heller & Fricke (2000) showed that the Hα flux of H II regions can contribute up to ∼40 per cent of the total Hα flux of a nearly well-resolved galaxy, but up to ∼75 per cent in the case where the spatial smoothing has been applied. This occurs because what used to be resolved H II regions have now become an H II complex due to the smoothing. Due to this, such unresolved H II complexes are likely host to a collection of smaller H II regions, but it has been found that it is more likely for the convolution of smaller H II regions to produce an even light distribution instead of a point source distribution appearing as a single H II region (Elmegreen et al. 2009, 2014). If DGs with intense star-forming regions are remnants of the same evolutionary phase that clump-clusters went through, it is not unrealistic for this H II complex to be dominated by a single H II region (alike to 30 Doradus). With clump-clusters' growth being dominated not by merging activity, but rather smooth gaseous inflow (Elmegreen et al. 2009), the high gas fraction and isolation of GAMA J141103.98−003242.3 strengthens the scenario of stochastic gravitational collapse as opposed to interaction triggered star formation.

The H II complex has a measured Hα luminosity of $10^{40.27}$ erg s^{-1}, velocity dispersion $\simeq 25$ km s^{-1} and a diameter of $\lesssim 600$ pc. This agrees with the scaling relations found by Wisnioski et al. (2012) for high-$z \sim L_*$ galaxies (e.g. clump-clusters; velocity dispersion ∝ radius ∝ Hα luminosity ∝ Jeans mass), even though the H II complex analysed here is hosted in a DG. In comparison to the work by Bauer et al. (2013), the SFR and SSFR of GAMA J141103.98−003242.3 including the H II complex are average for other galaxies of similar stellar mass. However, the SFR and SSFR of GAMA J141103.98−003242.3 excluding the H II complex are at the extreme lower bounds for the same mass bin. This hints at a case where the star formation in such DGs are typically dominated by a similar, single H II complex. Taking into account GAMA J141103.98−003242.3's high gas fraction, we conclude that even though this H II complex is significant for the galaxy itself (contributing 72 per cent of the total SFR of the galaxy), it is not currently experiencing a burst in its SFH where most of its stellar mass is formed. This is consistent with the work of Weisz et al. (2011), which found that DGs formed their underlying stellar population (accounting for ∼85 per cent of their stellar mass) prior to $z = 1$, with the rest of the stellar mass being formed by younger starbursts happening over the last 1 billion years.

These findings lead to the questions: 1. Where do the intense star-forming regions of DGs ($z \sim 0.001$–0.1) lie on known scaling relations of clump-clusters? 2. What fraction of DGs are undergoing extreme star formation in localized H II complexes and what is their duty cycle? These questions are outside the scope of this paper, but suit well to future analysis of a sample of DGs obtained with instruments such as SAMI,[3] KMOS[4] and MaNGA.[5] Considering the SAMI Galaxy Survey will observe ∼400 DGs over the next few years, it will be possible to rigorously test this sample for more galaxies like GAMA J141103.98−003242.3, in the pursuit

of understanding the SFH of DGs in the Local Universe and their place in the downsizing of star formation.

REFERENCES

Abazajian K. N. et al., 2009, ApJS, 182, 543
Allen J. T. et al., 2014, MNRAS, preprint (arXiv:1407.6068)
Barnes D. G. et al., 2001, MNRAS, 322, 486
Bauer A. E. et al., 2013, MNRAS, 434, 209
Begum A., Chengalur J. N., Karachentsev I. D., Sharina M. E., Kaisin S. S., 2008, MNRAS, 386, 1667
Bland-Hawthorn J. et al., 2011, Opt. Express, 19, 2649
Bosch G., Terlevich E., Terlevich R., 2009, AJ, 137, 3437
Bouchard A., Da Costa G. S., Jerjen H., 2009, AJ, 137, 3038
Bradley T. R., Knapen J. H., Beckman J. E., Folkes S. L., 2006, A&A, 459, L13
Brüns C. et al., 2005, A&A, 432, 45
Bruzual G., Charlot S., 2003, MNRAS, 344, 1000
Bryant J. J., Bland-Hawthorn J., Fogarty L. M. R., Lawrence J. S., Croom S. M., 2014a, MNRAS, 438, 869
Bryant J. J. et al., 2014b, MNRAS, preprint (arXiv:1407.7335)

---

[3] SAMI: http://sami-survey.org/
[4] KMOS: http://www.eso.org/sci/facilities/develop/instruments/kmos.html
[5] MaNGA: http://www.sdss3.org/future/manga.php

Cairós L. M., Vílchez J. M., González Pérez J. N., Iglesias-Páramo J., Caon N., 2001, ApJS, 133, 321

Cairós L. M., Caon N., Papaderos P., Kehrig C., Weilbacher P., Roth M. M., Zurita C., 2009, ApJ, 707, 1676

Cairós L. M., Caon N., García Lorenzo B., Kelz A., Roth M., Papaderos P., Streicher O., 2012, A&A, 547, A24

Cannon J. M., McClure-Griffiths N. M., Skillman E. D., Côté S., 2004, ApJ, 607, 274

Cappellari M., Emsellem E., 2004, PASP, 116, 138

Cardamone C. et al., 2009, MNRAS, 399, 1191

Cardelli J. A., Clayton G. C., Mathis J. S., 1989, ApJ, 345, 245

Croom S. M. et al., 2012, MNRAS, 421, 872

Dalcanton J. J., Williams B. F., Seth A. C. et al., 2009, ApJS, 183, 67

Díaz Á. I., 1998, Ap&SS, 263, 143

Dopita M. A. et al., 2006, ApJS, 167, 177

Dopita M. A., Sutherland R. S., Nicholls D. C., Kewley L. J., Vogt F. P. A., 2013, ApJS, 208, 10

Doran E. I. et al., 2013, A&A, 558, A134

Driver S. P. et al., 2011, MNRAS, 413, 971

Elmegreen B. G., Elmegreen D. M., Hirst A. C., 2004, ApJ, 612, 191

Elmegreen D. M., Elmegreen B. G., Marcus M. T., Shahinyan K., Yau A., Petersen M., 2009, ApJ, 701, 306

Elmegreen D. M. et al., 2014, ApJ, 787, L15

Faulkner D. J., 1967, MNRAS, 135, 401

Fontana A. et al., 2006, A&A, 459, 745

Garnett D. R., 1992, AJ, 103, 1330

Gerola H., Seiden P. E., Schulman L. S., 1980, ApJ, 242, 517

Gil de Paz A., Madore B. F., Pevunova O., 2003, ApJS, 147, 29

Gunawardhana M. L. P. et al., 2013, MNRAS, 433, 2764

Guseva N. G., Izotov Y. I., Stasińska G., Fricke K. J., Henkel C., Papaderos P., 2011, A&A, 529, A149

Hodge P. W., 1971, ARA&A, 9, 35

Hopkins A. M. et al., 2013, MNRAS, 430, 2047

Huang S., Haynes M. P., Giovanelli R., Brinchmann J., 2012, ApJ, 756, 113

Hughes T. M., Cortese L., Boselli A., Gavazzi G., Davies J. I., 2013, A&A, 550, A115

Hunter D. A., Hawley W. N., Gallagher J. S., III, 1993, AJ, 106, 1797

Hunter D. A., Elmegreen B. G., Ludka B. C., 2010, AJ, 139, 447

Izotov Y. I., Thuan T. X., 1999, ApJ, 511, 639

Izotov Y. I., Thuan T. X., 2004, ApJ, 602, 200

Izotov Y. I., Papaderos P., Guseva N. G., Fricke K. J., Thuan T. X., 2004, A&A, 421, 539

Izotov Y. I., Guseva N. G., Thuan T. X., 2011, ApJ, 728, 161

James B. L., Tsamis Y. G., Barlow M. J., Westmoquette M. S., Walsh J. R., Cuisinier F., Exter K. M., 2009, MNRAS, 398, 2

James B. L., Tsamis Y. G., Barlow M. J., 2010, MNRAS, 401, 759

Karthick M. C., López-Sánchez Á. R., Sahu D. K., Sanwal B. B., Bisht S., 2014, MNRAS, 439, 157

Kauffmann G. et al., 2003, MNRAS, 341, 33

Kelvin L. S. et al., 2012, MNRAS, 421, 1007

Kennicutt R. C., Jr, 1984, ApJ, 287, 116

Kennicutt R. C., Jr, 1998, ApJ, 498, 541

Kennicutt R. C., Jr, Lee J. C., Funes S. J., José G., Sakai S., Akiyama S., 2008, ApJS, 178, 247

Kewley L. J., Dopita M. A., 2002, ApJS, 142, 35

Kewley L. J., Dopita M. A., Sutherland R. S., Heisler C. A., Trevena J., 2001, ApJ, 556, 121

Kirby E. M., Jerjen H., Ryder S. D., Driver S. P., 2008, AJ, 136, 1866

Kobulnicky H. A., Kewley L. J., 2004, ApJ, 617, 240

Koribalski B. S., López-Sánchez Á. R., 2009, MNRAS, 400, 1749

Lada C. J., Muench A. A., Rathborne J., Alves J. F., Lombardi M., 2008, ApJ, 672, 410

Lee J. C. et al., 2009, ApJ, 706, 599

Leitherer C. et al., 1999, ApJS, 123, 3

Loose H.-H., Thuan T. X., 1986, ApJ, 309, 59

López-Sánchez Á. R., 2010, A&A, 521, A63

López-Sánchez Á. R., Esteban C., 2008, A&A, 491, 131

López-Sánchez A. R., Esteban C., 2009, A&A, 508, 615

López-Sánchez Á. R., Esteban C., 2010, A&A, 517, 85

López-Sánchez A. R., Koribalski B., van Eymeren J., Esteban C., Popping A., Hibbard J., 2010, ASP Conf. Ser. Vol. 421, Galaxies in Isolation: Exploring Nature Versus Nurture. Astron. Soc. Pac., San Francisco, p. 65

López-Sánchez Á. R., Mesa-Delgado A., López-Martín L., Esteban C., 2011, MNRAS, 411, 2076

López-Sánchez Á. R., Koribalski B. S., van Eymeren J., Esteban C., Kirby E., Jerjen H., Lonsdale N., 2012a, MNRAS, 419, 1051

López-Sánchez Á. R., Dopita M. A., Kewley L. J., Zahid H. J., Nicholls D. C., Scharwächter J., 2012b, MNRAS, 426, 2630

Markwardt C. B., 2009, ASP Conf. Ser. Vol. 411, Astronomical Data Analysis Software and Systems XVIII. Astron. Soc. Pac., San Francisco, p. 251

Mateo M. L., 1998, ARA&A, 36, 435

Mazzarella J. M., Boroson T. A., 1993, ApJS, 85, 27

McGaugh S. S., 1991, ApJ, 380, 140

Meurer G. R., Staveley-Smith L., Killeen N. E. B., 1998, MNRAS, 300, 705

Mollá M., García-Vargas M. L., Bressan A., 2009, MNRAS, 398, 451

Monreal-Ibero A., Vílchez J. M., Walsh J. R., Muñoz-Tuñón C., 2010, A&A, 517, A27

Morrissey P. et al., 2007, ApJS, 173, 682

Moustakas J., Kennicutt R. C., Jr, 2006, ApJS, 164, 81

Mühle S., Klein U., Wilcots E. M., Hüttemeister S., 2005, AJ, 130, 524

Nicholls D. C., Dopită M. ăA., Jerjenă H., Meureră G. ăR., 2011, AJ, 142, 83

Oey M. S., Clarke C. J., 1998, AJ, 115, 1543

Peimbert A., 2003, ApJ, 584, 735

Pérez-Montero E. et al., 2011, A&A, 532, A141

Pettini M., Pagel B. E. J., 2004, MNRAS, 348, L59

Pilyugin L. S., 2001a, A&A, 369, 594

Pilyugin L. S., 2001b, A&A, 374, 412

Pilyugin L. S., Thuan T. X., 2005, ApJ, 631, 231

Pleuss P. O., Heller C. H., Fricke K. J., 2000, A&A, 361, 913

Pustilnik S. A., Pramskij A. G., Kniazev A. Y., 2004, A&A, 425, 51

Salim S. et al., 2007, ApJS, 173, 267

Salpeter E. E., 1955, ApJ, 121, 161

Schaerer D., Vacca W. D., 1998, ApJ, 497, 618

Sharp R. et al., 2006, Proc. SPIE, 6269

Sharp R. et al., 2014, MNRAS, preprint (arXiv:1407.5237)

Storey P. J., Hummer D. G., 1995, MNRAS, 272, 41

Sweet S. M. et al., 2013, MNRAS, 433, 543

Tammann G. A., 1994, ESO Conference and Workshop Proceedings, Vol. 49, Garching, p. 3

Taylor E. N. et al., 2011, MNRAS, 418, 1587

Tolstoy E., Hill V., Tosi M., 2009, ARA&A, 47, 371

van Eymeren J., Koribalski B. S., López-Sánchez Á. R., Dettmar R.-J., Bomans D. J., 2010, MNRAS, 407, 113

Warren B. E., Jerjen H., Koribalski B. S., 2004, AJ, 128, 1152

Weisz D. R. et al., 2011, ApJ, 739, 5

Wisnioski E., Glazebrook K., Blake C., Poole G. B., Green A. W., Wyder T., Martin C., 2012, MNRAS, 422, 3339

Young T. et al., 2014, MNRAS, 444, 3052

Youngblood A. J., Hunter D. A., 1999, ApJ, 519, 55

APPENDIX A:

Table A1 compiles the dereddened line intensity ratios with respect to $I(\mathrm{H}\alpha) = 100$. Table A2 lists the results of the chemical abundance analysis for the H II complex discovered in the galaxy GAMA J141103.98−003242.3 and the centre of the galaxy. Table A3 compiles the oxygen abundances derived using the most commonly used strong emission-line methods.

Table A1. Dereddened line intensity ratios with respect to $I(H\beta) = 100$ for the H II complex discovered in the galaxy GAMA J141103.98−003242.3. The ionized gas observed in the rest of the galaxy is also presented. At the bottom of the table we also give the Hβ flux, the reddening coefficient, $c(H\beta)$, the equivalent widths of the absorption in the hydrogen lines, W_{abs}, and the equivalent widths of the emission H I Balmer lines. The value of $f(\lambda)$ considering the Cardelli, Clayton & Mathis (1989) extinction law and used for dereddening the line intensity ratios is also included. A colon denotes an error of larger than 40 per cent.

Line	$f(\lambda)$	H II complex	Rest of the galaxy
[O II] 3728	0.322	91.3 ± 5.6	352 ± 52
H11 3770	0.313	5.52 ± 0.42	. . .
[Ne III] 3869	0.291	60.4 ± 3.8	. . .
He I 3889 + H8	0.286	20.9 ± 2.2	. . .
[Ne III] 3969 + H7	0.267	36.7 ± 3.6	. . .
Hδ 4101	0.230	26.1 ± 2.0	25.0:
Hγ 4340	0.157	47.5 ± 2.3	43 ± 6.7
[O III] 4363	0.150	11.4 ± 0.8	. . .
He I 4471	0.116	3.87 ± 0.45	. . .
He II 4686	0.050	0.51:	. . .
[Ar IV] + He I 4712	0.043	1.72 ± 0.32	. . .
[Ar IV] 4740	0.034	0.99:	. . .
Hβ 4861	0.000	100.0 ± 3.6	100 ± 14
[O III] 4959	−0.025	234 ± 11	168 ± 23
[O III] 5007	−0.037	695 ± 30	482 ± 58
[O I] 6300	−0.262	1.70 ± 0.46	. . .
[S III] 6312	−0.264	1.73 ± 0.79	. . .
[O I] 6364	−0.271	0.78 ± 0.11	. . .
[N II] 6548	−0.295	1.75 ± 0.17	6.25:
Hα 6563	−0.297	279 ± 12	281 ± 34
[N II] 6583	−0.300	4.88 ± 0.29	16.7 ± 2.1
He I 6678	−0.312	3.17 ± 0.35	. . .
[S II] 6716	−0.318	7.67 ± 0.44	38.9 ± 4.7
[S II] 6731	−0.319	6.01 ± 0.35	24.6 ± 3.9
He I 7065	−0.364	2.74 ± 0.42	. . .
[Ar III] 7135	−0.373	10.33 ± 0.57	20.9 ± 3.8
EW(Hα) (Å)		451 ± 11	34.8 ± 3.2
EW(Hβ) (Å)		137 ± 4	6.8 ± 1.6
EW(Hγ) (Å)		44.2 ± 1.6	1.7 ± 0.4
EW(Hδ) (Å)		22.8 ± 0.9	1.1:
$F_{H\beta}$ $^\diamond$		22.6 ± 6.3†	9.4 ± 2.6†
$c(H\beta)$		0.34 ± 0.02	0.31 ± 0.04
W_{abs} (Å)		0.0 ± 0.1	0.8 ± 0.2

$^\diamond$ Units of 10^{-16} erg cm^{-2} s^{-1}.

† Error is currently dominated by a 28 per cent error in SAMI's absolute flux calibration, and in all values derived from it (see Allen et al. (2014) for more details).

Table A2. Physical conditions and chemical abundances of the ionized gas for the H II complex discovered in the galaxy GAMA J141103.98−003242.3 and the rest of the galaxy when this region is not considered. In this latter case, the electron temperatures were estimated as those that best reproduce the oxygen abundance computed via the SEL methods based on T_e. Bold values are those of most interest.

	H II complex	Rest of the galaxy
T_e[O III] (K)	14000 ± 650	12750 ± 1000
T_e[O II] (K)	12800 ± 450	11930 ± 800
n_e (cm^{-3})	140 ± 30	100
$12+\log(O^+/H^+)$	7.16 ± 0.07	7.85 ± 0.13
$12+\log(O^{++}/H^+)$	7.94 ± 0.05	7.90 ± 0.09
$12+\log(O/H)$	**8.01 ± 0.05**	**8.18 ± 0.11**
$\log(O^{++}/O^+)$	0.78 ± 0.09	0.05 ± 0.15
$12+\log(N^+/H^+)$	5.74 ± 0.05	6.35 ± 0.08
$12+\log(N/H)$	6.58 ± 0.09	6.67 ± 0.11
$\log(N/O)$	−1.43 ± 0.06	−1.51 ± 0.10
$12+\log(S^+/H^+)$	5.27 ± 0.04	5.99 ± 0.07
$12+\log(S^{++}/H^+)$	6.06 ± 0.18	. . .
$12+\log(S/H)$	6.27 ± 0.16	. . .
$\log(S/O)$	−1.74 ± 0.21	. . .
$12+\log(Ne^{++}/H^+)$	7.29 ± 0.06	. . .
$12+\log(Ne/H)$	7.36 ± 0.12	. . .
$\log(Ne/O)$	−0.65 ± 0.07	. . .
$12+\log(Ar^{++}/H^+)$	5.67 ± 0.06	6.06 ± 0.12
$12+\log(Ar^{+3}/H^+)$	5.00 ± 0.11	. . .
$12+\log(Ar/H)$	5.77 ± 0.07	5.90 ± 0.20
$\log(Ar/O)$	−2.24 ± 0.12	−2.29 ± 0.22
$c(H\beta)$	0.34 ± 0.02	0.31 ± 0.04
W_{abs} (Å)	0.0 ± 0.1	0.8 ± 0.2

Table A3. Oxygen abundances derived using the most commonly used strong emission-line methods. The strong emission-line calibrations are: M91: McGaugh (1991); KD02: Kewley & Dopita (2002); KK04: Kobulnicky & Kewley (2004); PT05: Pilyugin & Thuan (2005); P01: Pilyugin (2001a,b); PP04a: Pettini & Pagel (2004), using a linear fit to the N_2 parameter; PP04c: Pettini & Pagel (2004), using the O_3N_2 parameter. The last two columns list the average abundance value using all the empirical methods, the T_e method is not considered here. We provide two results: PPP, which considers the average value obtained with the PT05, P01, PP04a and PP04c calibrations and MKD, which assumes the average value of the M91, KD02, and KK04 calibrations. The typical uncertainty in these values is ∼0.10 dex. Bold values are those of most interest.

Parameters	$c(H\beta)$	W_{abs} (Å)	T_e	M91 R_{23}, y	KD02 R_{23}, y	KK04 R_{23}, y	PT05 R_{23}, P	P01 R_{23}, P	PP04a N_2	PP04c N_2O_3	Adopted MKD	PPP	Branch
H II complex	0.34 ± 0.02	0.0 ± 0.1	$\mathbf{8.01 \pm 0.05}$	8.17	8.33	8.35	7.99	7.88	7.90	7.90	**8.28**	**7.92**	Low
Rest of the galaxy	0.31 ± 0.04	0.8 ± 0.2	. . .	8.35	8.51	8.52	8.25	8.13	8.20	8.12	**8.45**	**8.18**	Intermediate
Difference	. . .	. . .	. . .	0.18	0.18	0.17	0.26	0.25	0.30	0.22	**0.18**	**0.26**	. . .

This paper has been typeset from a TeX/LaTeX file prepared by the author.